© 2015. Published by The Company of Biologists Ltd | Journal of Cell Science (2015) 128, 2293-2302 doi:10.1242/jcs.166249

RESEARCH ARTICLE

The myelin proteolipid plasmolipin forms oligomers and induces liquid-ordered membranes in the Golgi complex

Yakey Yaffe[1], Ilan Hugger[1], Inbar Nevo Yassaf[1], Jeanne Shepshelovitch[1], Ella H. Sklan[2], Yechiel Elkabetz[3], Adva Yeheskel[4], Metsada Pasmanik-Chor[4], Carola Benzing[5], Alexander Macmillan[6], Katharina Gaus[5], Yael Eshed-Eisenbach[7], Elior Peles[7] and Koret Hirschberg[1,*]

ABSTRACT

Myelin comprises a compactly stacked massive surface area of protein-poor thick membrane that insulates axons to allow fast signal propagation. Increasing levels of the myelin protein plasmolipin (PLLP) were correlated with post-natal myelination; however, its function is unknown. Here, the intracellular localization and dynamics of PLLP were characterized in primary glial and cultured cells using fluorescently labeled PLLP and antibodies against PLLP. PLLP localized to and recycled between the plasma membrane and the Golgi complex. In the Golgi complex, PLLP forms oligomers based on fluorescence resonance energy transfer (FRET) analyses. PLLP oligomers blocked Golgi to plasma membrane transport of the secretory protein vesicular stomatitis virus G protein (VSVG), but not of a VSVG mutant with an elongated transmembrane domain. Laurdan staining analysis showed that this block is associated with PLLP-induced proliferation of liquid-ordered membranes. These findings show the capacity of PLLP to assemble potential myelin membrane precursor domains at the Golgi complex through its oligomerization and ability to attract liquid-ordered lipids. These data support a model in which PLLP functions in myelin biogenesis through organization of myelin liquid-ordered membranes in the Golgi complex.

KEY WORDS: Plasmolipin, Golgi complex, Myelin

INTRODUCTION

Myelin comprises stacked, tightly layered membranes that surround axons multiple times. These membranes are essentially a very large domain within the surface membrane of oligodendrocytes and Schwann cells in the central and the peripheral nervous systems, respectively (Aggarwal et al., 2011a). Hence, each myelin-forming cell has to synthesize and later maintain the enormous mass of membranes that comprise the myelin sheath. The main function of myelin is to insulate axons and to limit Na^+ channels to distinct clusters known as nodes of Ranvier (Eshed-Eisenbach and Peles, 2013). This allows the rapid advance of action potential between the nodes. This structure of myelin is fundamental for the ability of the nervous system to rapidly process and respond to signals in a compact and dense environment. The fundamental importance of myelin is emphasized by the severe consequences of various demyelinating diseases, such as multiple sclerosis and other neuropathies (Simons et al., 2002). The lipid and protein composition of the myelin membrane is unique, although it has some similarities with epithelial apical membranes (Frank et al., 1998). Unlike most biological membranes, myelin is relatively protein poor (Aggarwal et al., 2011b). Myelin is highly enriched in sphingolipids and glycosphingolipids of the galactosylceramides and sulfatides species (Aggarwal et al., 2011a). Another key feature of myelin lipids is that the N-linked fatty acyl moieties are usually fully saturated and very long (22–26 carbon chains) (Yurlova et al., 2011). Myelin membranes are highly enriched with the plasmalogen form of phosphatidylethanolamine. These have been suggested to contribute to the rigidity of the myelin membrane, as well as to protect against fatty acid oxidation. A substantial proportion of myelin integral-membrane proteins are tetraspanning proteins. Of those, the most characterized are the myelin proteolipid protein PLP1, its splice variant DM20 (Van Dorsselaer et al., 1987), and the MARVEL-family proteins myelin and lymphocyte associated protein (MAL) and plasmolipin (PLLP) (Pérez et al., 1997). Like other MARVEL-family proteins, MAL and PLLP are also found in epithelial cells (Bosse et al., 2003). MAL is associated with the establishment and maintenance of the polarized phenotype in epithelial cells, among others. The mechanism of MAL function has been demonstrated to be the formation of membrane platforms through oligomerization and interaction with the surrounding membrane lipids (Magal et al., 2009), whereas the function of plasmolipin is essentially unknown. Sequence analysis shows 29% identity and 49% similarity between human PLLP and MAL. As in all other MARVEL proteins, PLLP is very hydrophobic because it partitions with lipid fractions in myelin tissue extracts. Increases in the postnatal levels of PLLP have been correlated with myelin development in both the central and peripheral nervous systems (Sapirstein et al., 1992a).

In this study, we test the hypothesis that the function of PLLP in myelin biogenesis is to generate myelin-precursor membrane domains in the Golgi complex. To this end, we expressed PLLP that had been tagged with fluorescent proteins in COS7 cells or primary Schwann cells co-cultured with neurons. We found that endogenous PLLP localized to the plasma membrane and the Golgi complex. Fluorescence recovery after photobleaching (FRAP) analysis demonstrated that PLLP recycled between the Golgi and the plasma membrane. FRET analysis indicated that PLLP formed oligomers, and mutagenesis of conserved aromatic amino acids within the MARVEL motif affected FRET efficiency. Co-expression of fluorescently tagged PLLP with the myelin proteolipid PLP1 revealed distinct segregation of these two proteins in the plasma membrane – PLP1 had a strong preference for sections of the plasma membrane with high curvature, from which PLLP was

[1]Department of Pathology, Sackler School of Medicine, Tel-Aviv 69978, Israel. [2]Department of Clinical Microbiology and Immunology, Sackler School of Medicine, Tel-Aviv 69978, Israel. [3]Department of Cell and Developmental Biology, Sackler School of Medicine, Tel-Aviv 69978, Israel. [4]Bioinformatics Unit, G.S.W. Faculty of Life Sciences, Tel-Aviv University, Tel-Aviv 69978, Israel. [5]EMBL Australia Node in Single Molecule Science, School of Medical Sciences and ARC Centre of Excellence in Advanced Molecular Imaging, Centre for Vascular Research University of New South Wales, Sydney, Australia 2033. [6]Biomedical Imaging Facility, University of New South Wales, Sydney, Australia 2033. [7]Department of Molecular Cell Biology, Weizmann Institute of Science, Rehovot, Israel 76100.

*Author for correspondence (koty@post.tau.ac.il)

Received 17 November 2014; Accepted 18 May 2015

Journal of Cell Science

Journal of Cell Science (2015) 128, 2293-2302 doi:10.1242/jcs.166249

almost excluded. Finally, expression of PLLP in COS7 cells blocked the secretory transport of vesicular stomatitis virus G protein (VSVG) at the Golgi entry stage but not of mutant VSVG that had an extended transmembrane domain. In polarized Madin-Darby canine kidney (MDCK) cells, this VSVG mutant was sorted to the apical membrane. Thus, we propose that PLLP functions in myelin biogenesis through the assembly of myelin liquid-ordered membrane domains at the Golgi complex.

RESULTS

The intracellular localization of PLLP

To characterize the intracellular localization of PLLP, a green fluorescent protein (GFP)-tagged version was inserted into the pMX retroviral vector. Retroviruses encoding PLLP–GFP were used to infect Schwann cells in a glia–neuron co-culture. Fig. 1A shows a 3-week-old culture, 10 days after the induction of myelin. Several PLLP–GFP-expressing elongated membrane structures were visible, some of which were co-labeled with myelin-associated glycoprotein (MAG), an early and non-compact myelin marker. A similar colocalization was observed by co-labeling for a compact myelin marker, myelin basic protein (MBP). Fig. 1B shows that in young co-cultures before myelin induction, PLLP–GFP was found in the plasma membrane, with a significant fraction localized to internal membranes. This fraction, at least in part, colocalized with the Golgi complex marker p115 (also known as USO1). We found that in COS7 cells, as well as in other cell types (data not shown), PLLP–GFP localized to the plasma membrane and the Golgi complex. To further confirm this localization, we used cyan fluorescent protein (CFP)-tagged galactosyltransferase (GalT–CFP), a marker for Golgi membranes (Zaal et al., 1999). Fig. 1C shows colocalization of PLLP–mCherry with GalT–CFP (Pearson's coefficient for the Golgi area only was 0.75). The cell surface PLLP fraction colocalized with Alexa-Fluor-488-modified cholera toxin B subunit.

Next, we examined the localization of endogenous PLLP. Fig. 2 shows the results of immunofluorescence analysis using an antibody specific to PLLP. Fig. 2A–C shows localization of PLLP to myelin membranes, as well as localization to p115-positive Golgi membranes. Localization to the Golgi was more prominent in undifferentiated Schwann cells. Also, staining of PLLP in myelin was seen at early stages of differentiation. MBP-positive myelin was strongly labeled for PLLP as well. Analysis of PLLP in sciatic nerve from a MAG–GFP transgene mouse showed colocalization of MAG and PLLP in a population of myelinated axons with smaller diameters (Fig. 2D). Moreover, the concentration of PLLP to structures associated with non-compact myelin is in line with the finding that PLLP localizes to zones of the myelin membrane that maintain the ability to be endocytosed.

A fraction of PLLP–GFP was found in dynamic tube-shaped membrane structures that seemed to follow microtubule tracks (Fig. 3A). These tube-shaped membranes depended on polymerized microtubules as they disappeared upon addition of nocodazole, a microtubule polymerization inhibitor. The tubular PLLP–GFP membrane structures did not colocalize with clathrin light chain (data not shown), early endosome antigen 1 (EEA1) or caveolin (Fig. 3B). However, some colocalization was observed with flotillin (Fig. 3C), a cytosolic plasma membrane peripheral protein that is associated with the formation of cholesterol-rich microdomains, as well as with a unique endocytic pathway (Glebov et al., 2006).

PLLP in the Golgi complex

We next attempted to elucidate the nature of the Golgi localization of PLLP–GFP. Therefore, we used FRAP to distinguish between the saturation of secretory transport due to overexpression and the steady-state localization due to recycling. PLLP–mCherry in the Golgi was photobleached in a cell co-expressing GalT–CFP. The Golgi-localized population of PLLP recovered within a time scale of 125 min based on the fit to an exponential equation (Fig. 4A,B). This time scale is comparable to that of overexpressed glucosylphosphatidylinositol (GPI)-anchored GFP, which has a plasma-membrane-to-Golgi recycling time of about 200 min (Nichols et al., 2001). Thus, the steady-state localization of PLLP to the Golgi is an outcome of its constant recycling from the plasma membrane.

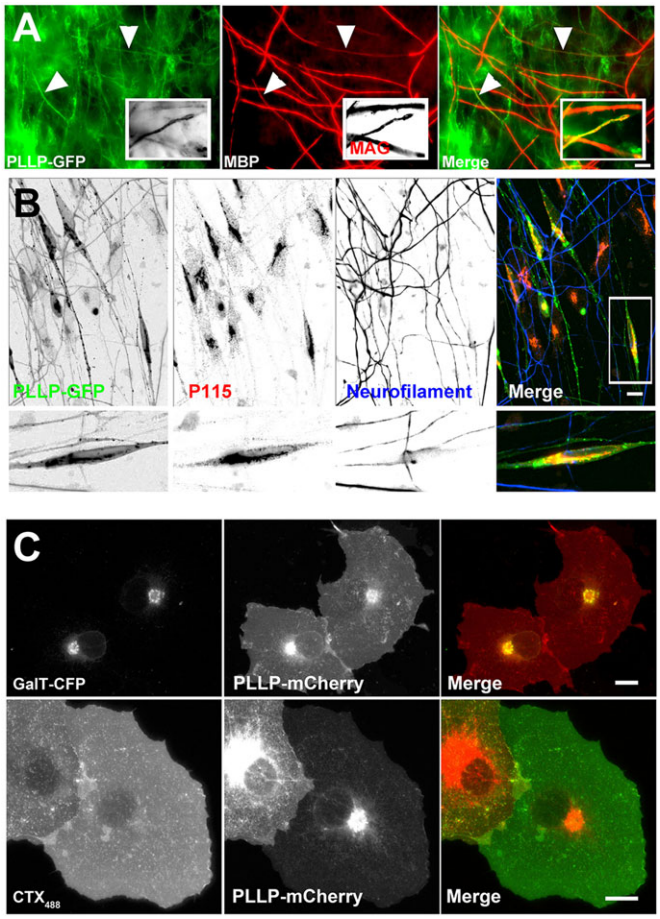

Fig. 1. The intracellular localization of fluorescently tagged PLLP. (A) Immunofluorescence analysis, 2 weeks after induction of myelin formation, of mouse Schwann cells co-cultured with neurons infected with the pMX retrovirus containing PLLP–GFP (green). Cells were fixed, permeabilized and labeled with primary antibodies against the early myelin marker MAG (red, inset) or MBP (red) and secondary fluorescently labeled antibodies, as described in the Materials and Methods. Arrowheads point to co-labeled myelin. (B) Immunofluorescence analysis of a mouse Schwann cell and neuron co-culture that had been infected with PLLP–GFP (green) without induction of myelin. Cells were fixed, permeabilized and labeled with antibodies against p115 (red in the merged image) or neurofilament (blue in the merged image). The inset in the merged image is shown in the lower panel magnified 2x. (C) Fluorescence microscopy analysis of cells co-expressing GalT–CFP (top left; green in the merged image) and PLLP–mCherry (middle; red in the merged image) or expressing PLLP–mCherry and labeled with Alexa-Fluor-488-modified cholera toxin B subunit (CTX_{488}, bottom left panel; green in the merged image). Scale bars: 10 µm.

PLLP and PLP1

Next, we compared the intracellular localization of PLLP with an abundant myelin protein, the myelin proteolipid PLP1. PLP1 is also a

Journal of Cell Science (2015) 128, 2293-2302 doi:10.1242/jcs.166249

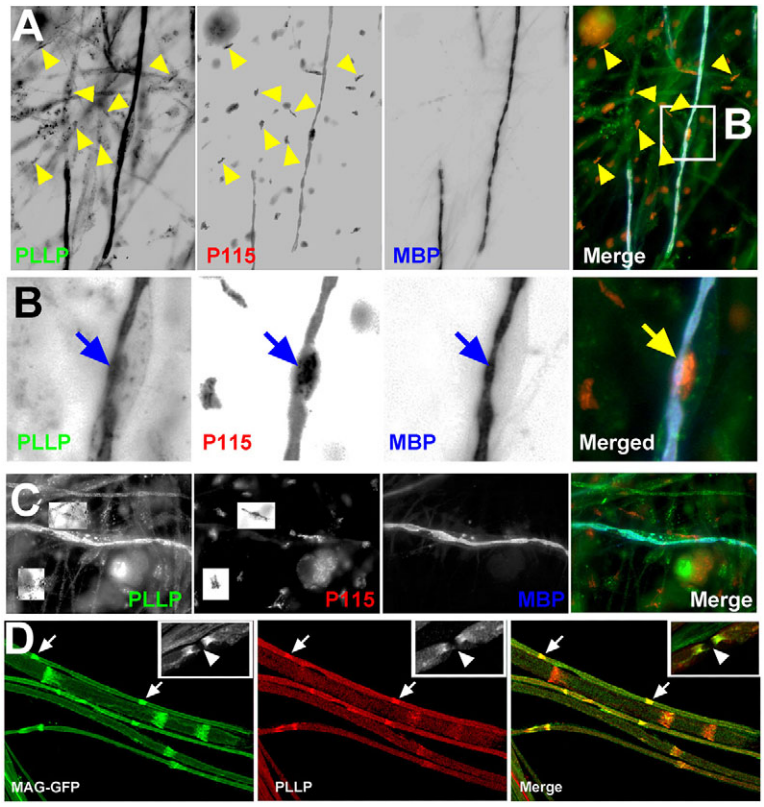

Fig. 2. The intracellular localization of endogenous PLLP. (A) Immunofluorescence analysis of mouse co-cultured Schwann cells and neurons at 2 weeks after the induction of myelin formation. Cells were fixed, permeabilized and labeled with primary antibodies against PLLP (green in the merged image), the Golgi marker p115 (red in the merged image), MBP (blue in the merged image) and secondary fluorescently labeled antibodies, as described in the Materials and Methods. The images for the separate channels are inverted. Arrowheads point to co-labeled Golgi membranes. The area within the rectangle is enlarged in B and arrows point to the Golgi complex. (C) Immunofluorescence analysis of mouse co-cultured Schwann cells and neurons as in A. The rectangles surrounding areas labeled for the Golgi marker p115 are inverted to show localization of endogenous PLLP in the Golgi complex. (D) Localization of PLLP in sciatic-nerve slices of a MAG–GFP (green) transgenic mouse that had been labeled as described in A with an anti-PLLP antibody (red). Arrows point to non-compact myelin structures (Schmidt–Lanterman incisures) co-labeled for MAG and PLLP. Arrowheads in insets point to paranodal loops.

tetraspanning protein that is found only in myelin. Like PLLP, PLP1 has been reported to partition to detergent-resistant membranes (Simons et al., 2002). Co-expression of PLLP and PLP1 resulted in both proteins efficiently arriving at the plasma membrane, although PLP1-positive intracellular membranes did not colocalize with PLLP (Fig. 5A). At the plasma membrane, PLLP and PLP1 displayed different preferences with regard to plasma membrane domains – PLLP was evenly distributed throughout the entire plasma membrane, whereas PLP1 concentrated at the contour of the cell, as well as in tubular plasma membrane protrusions. A line-scan analysis showed the specific increase of PLP1 concentration at the membrane and not of PLLP (Fig. 5B). The increase of PLP1 in the contour of the cell is clearly demonstrated in Fig. 5C. The partitioning of PLP1 to high-curvature plasma membrane areas was not facilitated by PLLP as it occurred when expressed alone or with other plasma membrane markers (data not shown). These data indicate that PLLP has no preference for high-curvature membranes, in contrast to that of PLP1.

Oligomerization of PLLP

Despite high levels of identity (29%) and similarity (47.8%) to human MAL and the similar localization of the two proteins to epithelial apical and myelin membranes, the intracellular localization of these proteins differs considerably. MAL localizes to the cell surface and to Rab11-positive endosomal sorting compartments, whereas PLLP localizes to the plasma membrane, a tubular endocytic compartment and the Golgi complex. Oligomerization plays an important role in the function of MAL. The propensity of MAL to form oligomers is, at least in part, facilitated by aromatic amino acids within ΦXXΦ motifs, which are known to mediate intra-membrane helix–helix interactions (Sal-Man et al., 2007). Interestingly, PLLP contains multiple ΦXXΦ motifs, as well as a high content of aromatic amino acid residues that are highly conserved throughout evolution (see alignment in Fig. 6A); therefore, we tested whether PLLP could form oligomers as well. To this end, we applied FRET analysis using a stepwise acceptor photobleaching technique. Principally, the acceptor protein is successively and moderately photobleached within a region of interest (ROI), and the fluorescence in the donor-fluorescence channel is recorded after every bleach cycle. As shown in Fig. 5B, a rectangular ROI over the Golgi complex was repeatedly photobleached in a cell expressing PLLP–GFP as the donor and PLLP–mCherry as the acceptor. The upper row shows the entire cell with the bleach box, and the two lower panels show the separate donor and acceptor channels. The increase in fluorescence observed post bleach in the donor channel is indicative of FRET. Fig. 6C shows a typical quantitative analysis of the donor and acceptor FRET efficiency, and acceptor residual fluorescence values. To demonstrate that the FRET is not an artifact of the formaldehyde fixation, we performed FRET experiments in living unfixed cells (Fig. 6D); similar FRET values were obtained for both fixed and unfixed cells. However, it was difficult to perform a reproducible quantitative analysis in living unfixed cells owing to the fast membrane diffusion. These data demonstrate the self-association of PLLP. To demonstrate that the FRET interaction represents specific interactions and is not a result of simple crowding of donor and acceptor molecules, we compared the FRET efficiency of PLLP pairs with PLLP and either VSVG or a VSVG mutant with an extra four amino acids added to its transmembrane domain (VSVGIn4; Magal et al., 2009) (Fig. 6E). The FRET efficiency of PLLP with VSVG was more than an order of magnitude lower than that of PLLP donor and acceptor pairs. For PLLP and VSVGIn4, FRET efficiency was higher than that with VSVG but still approximately sixfold lower than that of PLLP pairs. These data suggest that the FRET between PLLP donors and acceptors denotes specific interactions.

In MAL, elimination of ΦXXΦ motifs using mutagenesis results in a significant decrease in oligomerization (Magal et al.,

Journal of Cell Science (2015) 128, 2293-2302 doi:10.1242/jcs.166249

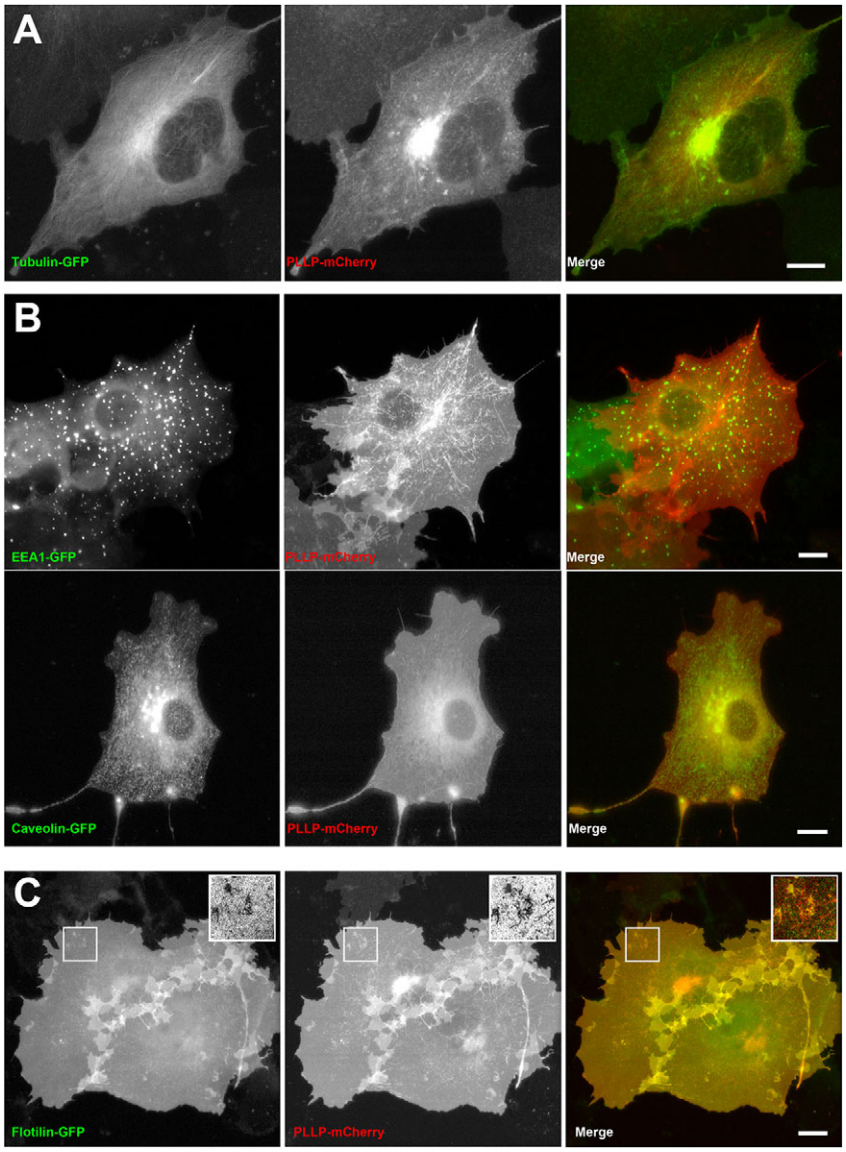

Fig. 3. Characterization of the tubular endocytic compartment marked by fluorescently tagged PLLP. (A) The PLLP-labeled tubular endocytic compartment is aligned with polymerized microtubules. A living cell co-transfected with tubulin–GFP (green in the merged image) and PLLP–mCherry (red in the merged image). (B) Colocalization of PLLP–mCherry (red in the merged image) with GFP-tagged EEA1 (green in the merged image; top panel; Pearson's colocalization coefficient 0.42) or caveolin (green in the merged image; bottom panel; Pearson's colocalization coefficient 0.87). (C) Co-expression of PLLP–mCherry (red in the merged image) with flotillin–GFP (green in the merged image); Pearson's colocalization coefficient 0.87. Insets are enlarged and inverted images of the boxed areas, which show colocalization. Scale bars: 10 µm. The control for Pearson's coefficient was co-expressed PLLP–mCherry and PLLP–GFP (0.98).

2009), whereas mutagenesis of aromatic amino acids in the MARVEL motif of occludin has a small effect on oligomerization (Yaffe et al., 2012). We therefore tested whether PLLP oligomerization is facilitated by aromatic amino acids. Fig. 6F shows a predicted structural model of PLLP, which was generated using the Rosseta software package. Two mutant proteins were generated, each with a set of four aromatic amino acids mutated to alanine residues (labeled yellow and red in Fig. 6F). The mutant marked M1 in Fig. 6G contains mutations in two pairs of conserved ΦXXΦ motifs: W68A–F71A and Y162A–W165A (Fig. 6F, amino acids in yellow). The mutant M2 (Fig. 6G) contained mutations in four conserved yet scattered aromatic amino acids – W52A, F75A, F119A, F146A (Fig. 6F, red). FRET analysis between a wild-type donor or acceptor and a mutant acceptor or donor, respectively, was performed. FRET efficiency was reduced by 20% and 60% for pairs comprising wild type and either M1 or M2, respectively. Surprisingly, FRET efficiency of an M1 mutant donor and an M1 mutant acceptor pair was about 60% higher than control. A plausible explanation is that the mutated ΦXXΦ aromatic amino acids are pointed outwards. Consequently, they contribute to the oligomerization interaction, but at the same time impede direct helix–helix contact. In other words, the absence of the motifs in both donor and acceptor (M1–M1) resulted in a tighter conformation of oligomerization, yielding higher FRET efficiency values. These data establish that PLLP oligomers form at the Golgi and the plasma membrane.

PLLP induces liquid-ordered membranes in the Golgi complex

We have previously shown that a direct consequence of oligomerization of MARVEL proteins is the formation and stabilization of liquid-ordered thick membrane domains (Aranda et al., 2011; Magal et al., 2009). Thus, we questioned whether PLLP oligomerization affects the membrane environment of the Golgi complex. To this end, we followed the secretory transport of the thermoreversible VSVG mutant VSVGtsO45 (Hirschberg et al., 1998; Presley et al., 1997), which is tagged with yellow fluorescent protein (VSVGtsO45–YFP), in cells co-expressing PLLP. VSVG is a transport-competent membrane protein that is excluded from liquid-ordered domains, as well as from membranes that are resistant to Triton X-100 detergent (Dukhovny et al., 2006; van Meer and Simons, 1982), and it is targeted to the basolateral membrane in

Journal of Cell Science (2015) 128, 2293-2302 doi:10.1242/jcs.166249

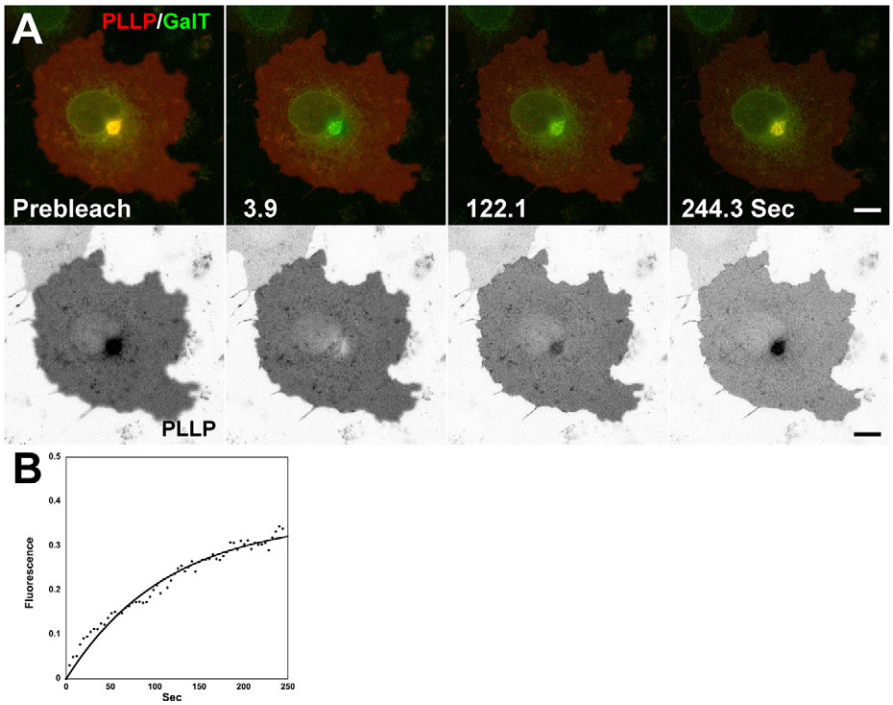

Fig. 4. Cycling of fluorescently tagged PLLP between the plasma membrane and the Golgi complex. (A) FRAP of PLLP–mCherry in the Golgi complex of a cell co-expressing GalT–CFP (green) and PLLP–mCherry (red and inverted lower panel). Scale bars: 10 µm. (B) Quantitative analysis of the recovery of PLLP–mCherry. Average fluorescence intensity data (dots) was fitted with a single exponential equation $Fi = Mf \times (1 - e^{-kt})$. The time constant was 2.08 min.

polarized epithelia. After overnight accumulation in the endoplasmic reticulum (ER) membranes at the non-permissive temperature of 39.5° C, cells were transferred to the permissive temperature (32°C). At this temperature, VSVG folds properly, leading to its release from the ER. As shown in Fig. 7A and in supplementary material Movies 1 and 2, in cells co-expressing PLLP, VSVG–YFP was completely blocked from passing through the Golgi for secretory transport. As a consequence, VSVG accumulated in membranes at the Golgi circumference, as well as in pre-Golgi compartments (Fig. 7B,C). This was confirmed by quantitative analysis of the fluorescence intensity of the Golgi. In a cell that did not express PLLP, a clear peak of VSVG was seen approximately 20 min after the beginning of the experiment. However, in a cell that did express PLLP, the fluorescence intensity in the Golgi accumulated and did not decline for the duration of the

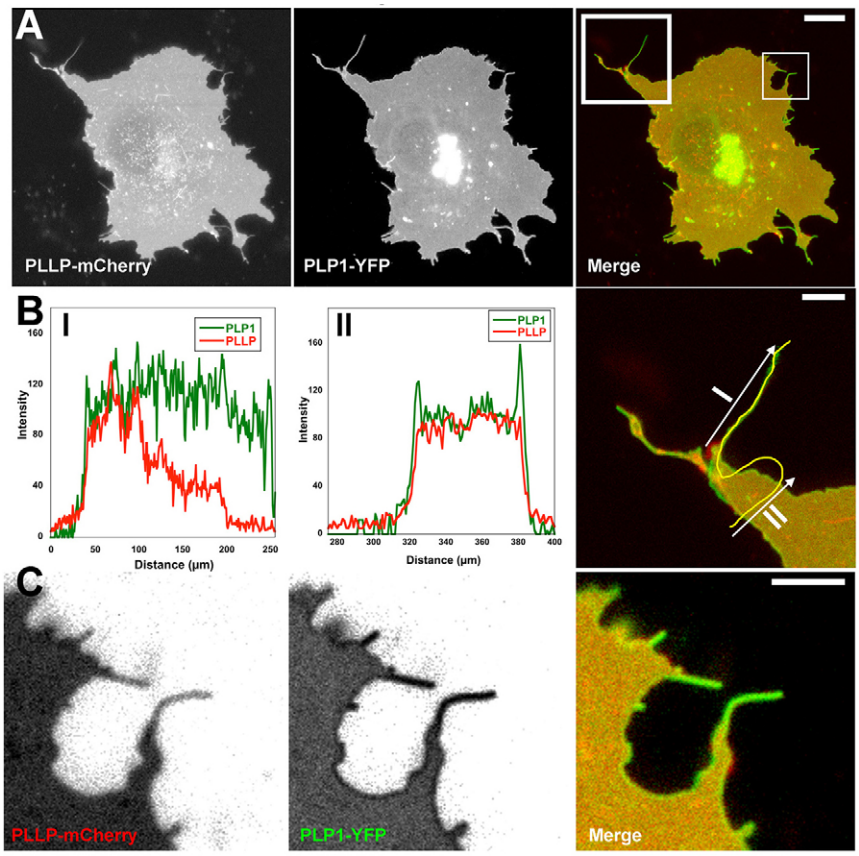

Fig. 5. Partitioning at the plasma membrane of the myelin proteolipids PLLP and PLP1. (A) Segregation at the plasma membrane of PLLP and PLP1. Co-expression of PLLP–mCherry (red) and PLP1–YFP (green) in COS7 cells. (B) PLP1–YFP and not PLLP–mCherry partitioned into high-curvature plasma membrane edges. Line-scan analysis of the intensity of PLLP–mCherry (red line) and PLP1–YFP (green line) fluorescence. Graphs I and II correspond to lines I and II in the enlarged inset from A. (C) An enlarged inset from A showing the actual concentration of PLP1 at the rims and tubes of the plasma membrane. Scale bars: 10 µm (A); 3 µm (B,C).

Journal of Cell Science (2015) 128, 2293-2302 doi:10.1242/jcs.166249

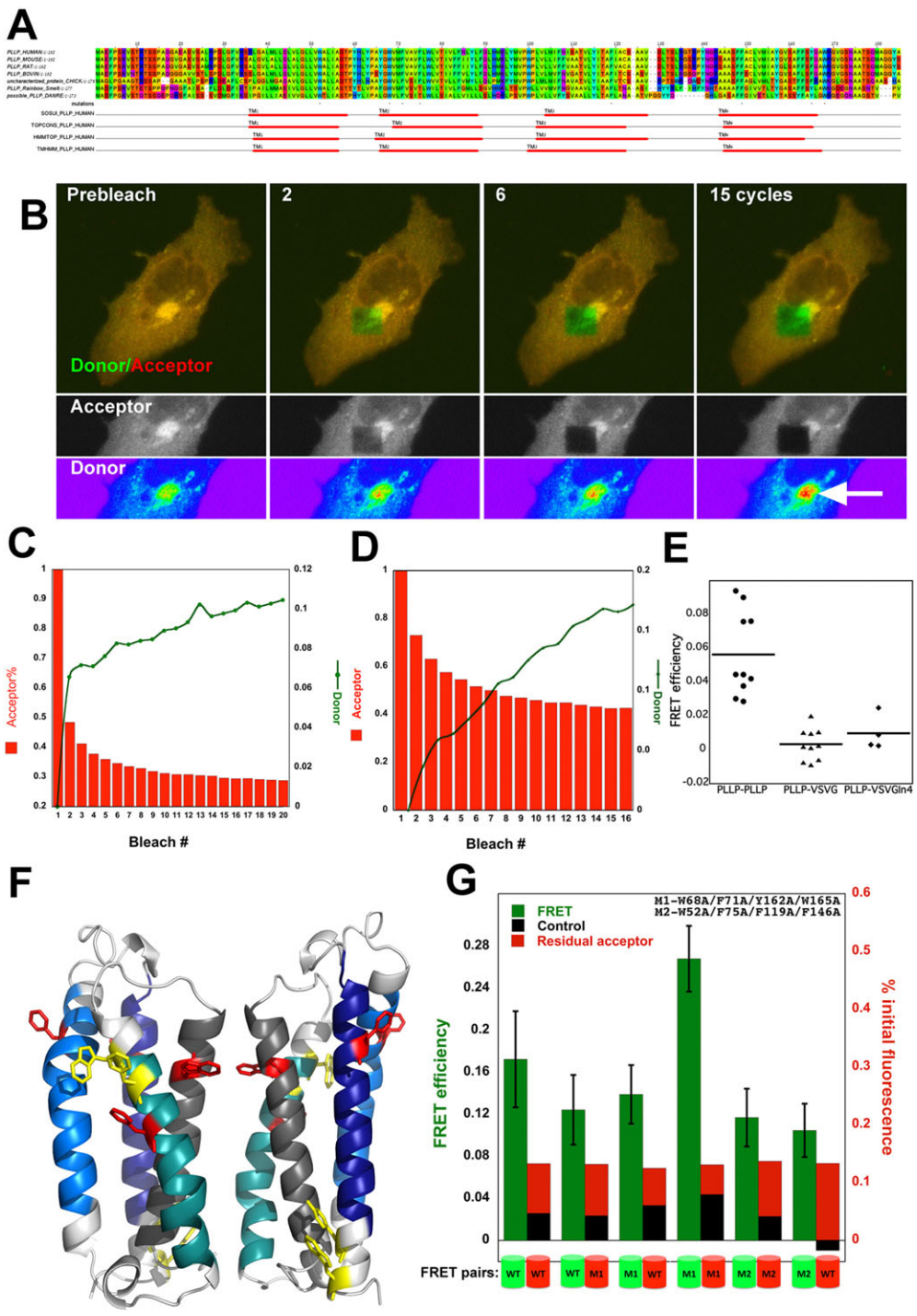

Fig. 6. Oligomerization of PLLP in the Golgi complex. (A) Sequence alignment and transmembrane domain (TMD) predictions of PLLP proteins – seven PLLP paralogs were aligned by multiple sequence alignment and color-coded according to the amino acid charge groups. Transmembrane (TM1–4) helix predictions for the human PLLP sequence were obtained by using four different webservers (red lines under the alignment). (B) Stepwise acceptor photobleaching to detect FRET between PLLP tagged with GFP (green) and mCherry. The top panel is a typical cell showing the bleached rectangle (green). Donor and acceptor channels are separated and shown in the middle and lower panels, respectively. The arrow points to an area of increased fluorescence, demonstrating FRET. (C) Quantification of a typical FRET experiment. Red columns are the fraction of residual fluorescence intensity of the bleached acceptor. Green dots and line are the calculated FRET efficiency. (D) Same as in C, except that the experiment was performed on a living unfixed cell. (E) Specificity of FRET between PLLP molecules. Dot-plot analysis of FRET efficiency between overexpressed proteins at the plasma membrane. FRET was measured as described for PLLP–YFP and PLLP–mCherry (filled circles, *n*=10), VSVG–YFP and PLLP–mCherry (filled triangles, *n*=10) and VSVGln4–YFP and PLLP–mCherry (filled diamonds, *n*=4). (F) The initial determination of the structure of human PLLP – TM1, gray; TM2, cyan; TM3, blue; TM4, dark blue. Point mutations W68A, F71A, Y162A and W165A are indicated as yellow sticks; point mutations (from aromatic amino acids to alanine) W52A, F75A, F119A and F146A are indicated as red sticks. (G) The effect of mutagenesis of two mutant PLLP molecules (M1 comprises mutation of the residues labeled in yellow in panel F; M2 comprises mutation of the residues labeled in red in panel F) on the FRET efficiency between GFP- and mCherry-tagged PLLP. In each mutant, four aromatic amino acids were replaced by alanine. Data shown is average±s.d. (*n*=10–12). FRET efficiency is calculated as described in the Materials and Methods. Green columns represent FRET efficiency. Black columns represent control FRET efficiency outside of the bleached area and red columns represent average residual acceptor.

Journal of Cell Science (2015) 128, 2293-2302 doi:10.1242/jcs.166249

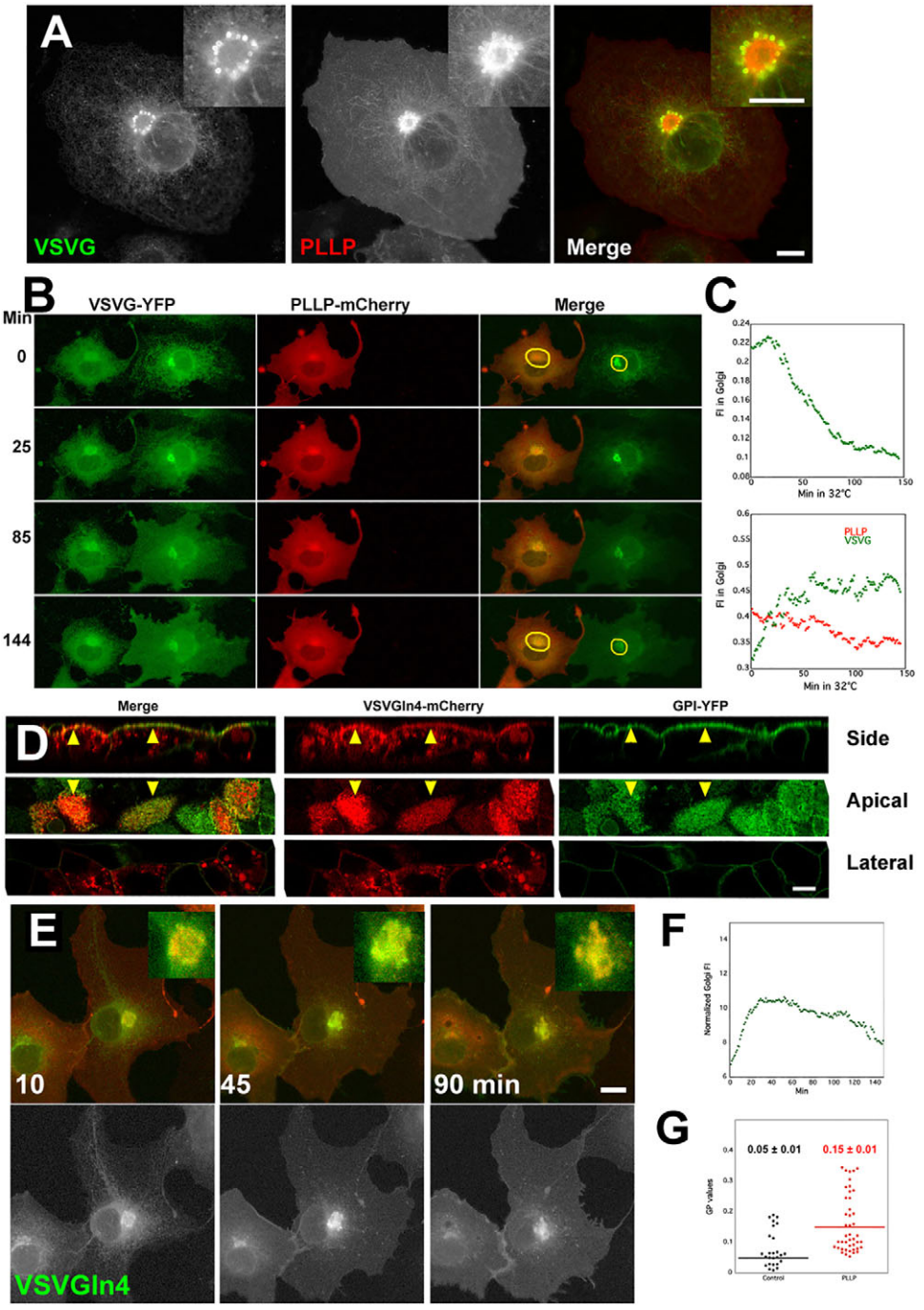

Fig. 7. PLLP blocks Golgi-to-plasma-membrane transport of VSVG but not transport of VSVGln4, which has a longer transmembrane domain, by inducing proliferation of liquid-ordered membranes. (A) VSVG–YFP accumulates at the Golgi periphery in PLLP–mCherry-expressing cells. VSVG–YFP (green) and PLLP–mCherry (red) were co-expressed in COS7 cells. Cells were imaged after overnight incubation at 39.5°C to allow accumulation of VSVG in the ER and then shifted to 32°C. A single image from the time-lapse sequence in supplementary material Movie 1 is shown. (B) Golgi-to-plasma-membrane transport of VSVG–YFP (green) is blocked in cells expressing PLLP–mCherry (red). Time-lapse analysis of a living cell expressing VSVG–YFP with or without co-expression of PLLP–mCherry (time-lapse sequence of supplementary material Movie 2). The intensity of fluorescence in the yellow circles surrounding the Golgi complex in each cell is shown in C. The top graph is the left-hand cell that did not express PLLP and the bottom graph represents the cell co-expressing PLLP–mCherry. (D) The VSVGln4–mCherry mutant with an elongated transmembrane domain is sorted to the apical membrane in polarized MDCK cells. VSVGln4–mCherry (red) was expressed in filter-grown polarized MDCK cells that stably expressed the apical marker GPI–YFP (green). A three-dimensional reconstruction with three sections *yz* (side) and *xy* at the apical and lateral plains. Arrowheads point to the apical PM. (E) Secretory transport of VSVGln4–mCherry is not blocked by PLLP–mCherry. Co-expression of VSVGln4–YFP (green) and PLLP–mCherry (red). Selected images from a time-lapse sequence (supplementary material Movie 3) at the designated times after the shift from 39.5°C to 32°C. The bottom panel shows VSVG moving from the ER through the Golgi to the plasma membrane. (F) Quantification of the Golgi fluorescence shown in E. (G) Analysis of membrane order using Laurdan analysis. COS7 cells expressing (red filled circles) or not expressing (black filled circles) PLLP–mCherry were labeled with Laurdan, imaged and processed as described in the Materials and Methods. Horizontal lines represent the mean and values are mean± s.e.m. Scale bars: 10 µm (A,D,E).

experiment (Fig. 7C). Throughout the experiment, VSVG remained at this location and did not arrive at the plasma membrane. We hypothesized that PLLP oligomerization and accumulation in the Golgi, as well as its association with lipids, creates a thick liquid-ordered lipid environment, which blocks the passage of VSVG.

VSVG is targeted to the basolateral plasma membrane pole in polarized MDCK cells (Compton et al., 1989; Thomas et al., 1993). We thus asked if elongation of the VSVG transmembrane domain with four hydrophobic amino acids (VSVGln4) would allow it to partition into thick liquid-ordered membrane domains in the Golgi, thereby redirecting it to the apical plasma membrane instead of the basolateral plasma membrane domain in polarized epithelia. To this end, the sorting of VSVGln4 was tested in polarized MDCK cells grown on Transwell filters. Fig. 7D shows that, in a MDCK cell line that stably expressed the apical marker GPI–YFP, VSVGln4 colocalized with GPI–YFP at the apical plasma membrane domain. Next, we tested our hypothesis that PLLP induces the proliferation of thick liquid-ordered lipid domains by analyzing its effect on the secretory transport of VSVGln4. We anticipated that PLLP-mediated proliferation of liquid-ordered domains would not block the transport of VSVGln4. The effect of PLLP on VSVGln4 is shown in Fig. 6E,F, as well as in supplementary material Movie 3. Unlike wild-type VSVG, VSVGln4 effectively moved through the Golgi complex despite the presence of PLLP in the Golgi. To rule out that the effect was a result of different levels of PLLP in the Golgi, VSVG–CFP and VSVGln4–YFP were co-expressed in PLLP–mCherry-expressing

Journal of Cell Science

Journal of Cell Science (2015) 128, 2293-2302 doi:10.1242/jcs.166249

cells. Supplementary material Fig. S1A shows that VSVG was restricted to the periphery of the Golgi complex, whereas VSVGIn4 and PLLP overlapped with all Golgi membranes. Supplementary material Fig. S1B shows the Pearson coefficient values for all of the paired combinations of the three proteins. Here, the coefficients were obtained for the Golgi ROI; PLLP and VSVGIn4 had a high value of 0.83–0.89 for the duration of the experiment.

Finally, to demonstrate that the PLLP-mediated block of VSVG was through the induction of liquid-ordered membranes, we performed staining with the Laurdan dye to observe changes in the degree of order of Golgi membranes. Fig. 7G shows that, in PLLP–mCherry-expressing cells, a significant increase in the generalized polarization values for Golgi membrane (from 0.05±0.01 to 0.15±0.01, mean±s.e.m.) was observed.

In summary, we propose that the self-association and induction of liquid-ordered membrane domains in the Golgi complex point to PLLP as a key protein in myelin membrane biogenesis. In the Golgi complex, PLLP assembles myelin membrane domains that are to be delivered as membrane carriers to the rapidly growing myelin.

DISCUSSION

PLLP is a typical MARVEL protein – it is small, hydrophobic, has four transmembrane-spanning helices, a high content of conserved aromatic amino acids (some in ΦXXΦ motifs), forms oligomers, and associates with and attracts liquid-ordered lipids. All of these attributes, as well as PLLP's high similarity to MAL and its expression in myelin and epithelia, suggest that PLLP contributes to the generation of functional protein–lipid membrane domains. We propose that PLLP forms oligomers at the Golgi complex and attracts liquid-ordered lipids, such as cholesterols and long saturated fatty-acyl-chain sphingolipids. In Schwann cells, these protein–lipid domains are essentially myelin membrane domains. These are then delivered to the cell surface, creating the massive flux of membranes that is required during myelin biogenesis. PLLP is then recycled to the Golgi complex for additional rounds of myelin membrane domain assembly and delivery. Another non-exclusive proposed function might be that PLLP is a sensor of myelin membrane thickness, as has been suggested for MAL (Magal et al., 2009; Mitra et al., 2004).

Myelin proteolipids were discovered over 60 years ago (Folch and Lees, 1951). One myelin proteolipid was later named lipophilin (Boggs and Moscarello, 1978) and then PLP1 after the sequencing of the gene (Naismith et al., 1985). PLLP was primarily identified in kidney samples and was then found to be a myelin proteolipid protein (Cochary et al., 1990). Despite all of the data accumulated, very little is known about the function of PLLP or any other proteolipid in myelin biogenesis. Here, we used expression of fluorescently labeled PLLP in both COS7 cells and in primary Schwann-cell–neuron co-cultures. The latter allows induction of myelin formation and the specific expression of proteins in the Schwann cells using retroviral vectors. PLLP is mainly a plasma membrane protein that recycles through Golgi membranes through a tubular endocytic organelle. Its recycling from the plasma membrane is supported by the findings that it serves as a mouse viral receptor (Miller et al., 2008) and that it co-fractionates with endocytic markers (Sapirstein et al., 1992b). Recently PLLP has been demonstrated to regulate epithelial development through the regulation of endocytosis in zebrafish (Rodríguez-Fraticelli et al., 2015). Labeling of the Golgi was apparent in young Schwann cells and, to a lesser extent, in older cultures. It is conceivable that the recycling in the Golgi is more intense during myelin biogenesis and less intense during its maintenance. Another explanation could be that the Golgi population of fluorescently tagged PLLP is masked by the bright plasma membrane fluorescence. Nevertheless, the pattern of recycling in the Golgi of PLLP is a hallmark of a protein that is associated with orchestrating a biosynthetic flux of membrane. The partial colocalization of PLLP with flotillin could suggest a non-clathrin, non-caveolin plasma-membrane-to-Golgi pathway (Otto and Nichols, 2011). Flotillin binds to the inner leaflet of cholesterol-rich membrane domains. Thus, the interaction with a MARVEL-family protein is conceivable.

Oligomer formation has been demonstrated in this work by using FRET. In the case of PLLP, the FRET signal was rather strong. Oligomerization of MARVEL proteins might be driven, at least in part, by hydrophobic mismatching interactions between transmembrane domains and fatty acyl chains of lipids (Milovanovic et al., 2015). However, it has been shown that an intrinsic propensity to self-associate is a prerequisite for mismatch-driven oligomerization. We have previously shown this through mutagenesis of MAL and modifications of the lipid content by the addition of cholesterol, as well as short and extra-long chain ceramides, to MAL's surrounding membrane (Magal et al., 2009). Here, we show that mutagenesis of conserved aromatic amino acids affects the oligomerization. The attraction of lipids with long and saturated fatty acyl chains, promoting liquid-ordered membrane formation, is another way in which integral membrane proteins reduce the hydrophobic mismatch-driven tension. Thus, the final product of mismatch-driven oligomerization and the attraction of distinct lipid species is the formation of a large and stable membrane domain that might have various biological functions. PLLP expression in COS7 cells resulted in a significant proliferation of liquid-ordered membranes that led to the blocking of the transport of VSVG–YFP through the Golgi complex. This was shown by elongating the VSVG transmembrane domain with four amino acids, which eliminated the block. Thus, we assert that PLLP recycling, oligomerization and proliferation of liquid-ordered membranes in the Golgi provides evidence to support the function of PLLP in myelin biogenesis, a process in which massive amounts of membrane are synthesized, sorted and delivered.

Co-expression of PLLP with PLP1 demonstrated distinct distribution of the two proteins within the plasma membrane. It has been reported that, as for PLLP, PLP1 can be isolated in detergent-resistant membranes (Schneider et al., 2005). PLP1 and PLLP are mainly plasma membrane proteins in COS7 cells; however, at the cell surface, they clearly segregate at the contour of the cell, where PLP1 is enriched. Tubular plasma membrane protrusions were dominated by high concentrations of PLP1 and reduced concentrations of PLLP. Membrane tubes and the contour of the cell have increased levels of curvature compared with the near zero curvature of the COS7 flat plasma membrane. This partitioning of PLP1 was independent of PLLP. Despite the identical topology of PLP1 to that of PLLP, the two proteins have no sequence similarity. The function of the myelin proteolipid PLP1 is also unknown; however, partitioning of PLP1 to high-curvature plasma membrane zones suggests that it has a role in the stabilization of tightly rolled myelin sheets or, alternatively, in the stabilization of distinct myelin high-curvature subdomains. Nevertheless, the function of PLP1 is distinct from that of PLLP. An exciting hypothesis that can be tested is that the tetraspanning myelin proteins PLLP and PLP1 function to establish the composition and the shape of myelin, respectively.

MATERIALS AND METHODS

Reagents and constructs

PLLP–GFP was kindly provided by Miguel Angel Alonso (Centro de Biologia Molecular 'Severo Ochoa', Madrid). Human plasmolipin (accession number NP_057077) was subcloned into pmCherry-C1, pECer-C1 or pEYFP-C1 (Clontech) using *Bsp*EI and *Bam*HI restriction sites and verified by sequencing.

Journal of Cell Science (2015) 128, 2293-2302 doi:10.1242/jcs.166249

Cell culture and transfections

To produce clones stably expressing mCherry–PLLP, 10 µg of the neomycin-resistance-containing expression constructs were transfected into MDCK cells using Lipofectamine 2000. Selection medium containing 0.8 mg/ml G418 (Gibco) was added 48 h after transfection. The cells were incubated with sodium butyrate for 2 to 6 h before the experiment. MDCK cells stably expressing mCherry–PLLP were grown on Transwell filters (Corning) for 4 to 12 days.

Dissociated dorsal root ganglia cultures were prepared from rat embryos at day 15.5 of gestation. Dorsal root ganglia were dissociated and plated at a density of 4×10^4 per 13-mm slide, coated with Matrigel (BD Biosciences) and poly-L-lysine (Sigma). A day after plating, cultures were incubated with retrovirus-containing medium supplemented with 5 µg/ml polybrene (Sigma) for 2 h, for three consecutive days. During the first two days after plating, cultures were grown in neurobasal medium (Sigma) supplemented with B-27, glutamax, penicillin-streptomycin (all from Gibco) and 50 ng/ml nerve growth factor (NGF, Alomone Labs). Cultures were then grown for eight additional days in BN medium containing Basal Medium Eagle (Sigma), insulin, transferrin and selenium (ITS) supplement (Sigma), glutamax (Gibco), 0.2% bovine serum albumin (BSA, Sigma), 4 mg/ml D-glucose (Sigma), 50 ng/ml NGF and antibiotics. To induce myelination, cultures were grown in BNC medium, namely a BN medium supplemented with 15% heat-inactivated fetal calf serum (replacing BSA) and 50 µg/ml L-ascorbic acid (Sigma). After ten additional days, cultures were fixed with 4% paraformaldehyde (PFA) for 10 min at room temperature.

Retrovirus production

cDNA encoding PLLP–GFP was subcloned into pMX-EGFP (Clontech), excluding the EGFP cassette. For retroviral stock preparation, helper-virus-free Phoenix-Eco packaging cells were transfected with the pMX-PLLP–GFP construct using the $CaPO_4$ method. Medium was changed 1 day after transfection and collected after an additional 24 h. Virus-containing media were centrifuged to remove cells and stored at −80°C until use.

Immunofluorescent labeling

Fixed cultures were permeabilized in methanol for 5 min at −20°C. Following three washes in PBS, cultures were incubated in blocking solution (PBS, 1% glycine, 5% normal goat serum, 0.1% Triton X-100) for 45 min at room temperature. Cultures were subsequently incubated overnight at 4°C with primary antibodies diluted in blocking solution. After extensive washing with PBS, cultures were incubated with fluorophore-conjugated secondary antibodies for 45 min at room temperature, and were then washed and mounted in elvanol (DuPont). Primary antibodies used were: rabbit anti-PLLP (Abcam); rat anti-MBP, rat anti-neurofilament-H, mouse anti-MAG (Merck Millipore). Secondary antibodies were Alexa-Fluor-647-conjugated donkey anti-rat-IgG and Cy3-conjugated donkey anti-mouse-IgG (Jackson ImmmunoResearch Laboratories).

Confocal microscopy, time-lapse imaging, FRAP analysis and image processing

Cells were imaged in Dulbecco's modified Eagle's medium (DMEM) without Phenol Red but with supplements, including 20 mM HEPES, pH 7.4, or with Hybernate A medium (Gibco). Transfection and imaging were performed in Lab-Tek chamber slides (Nunc). Fluorescence images were obtained using a confocal microscope (LSM model PASCAL or 510 META with an Axiovert 200 microscope; Carl Zeiss MicroImaging). Fluorescence emissions resulting from argon 458-nm, 488-nm, 514-nm and 543-nm laser lines for enhanced (E)CFP, EGFP, EYFP and mCherry, respectively, were detected using filter sets supplied by the manufacturer. The confocal and time-lapse images were captured using a Plan-Apochromat 63° – NA 1.4 objective (Carl Zeiss MicroImaging). Image capture was performed using the standard time-series option (Carl Zeiss MicroImaging). The temperature on the microscope stage was monitored during time-lapse sessions using an electronic temperature-controlled airstream incubator. Images and movies were generated and analyzed using the Zeiss LSM software and ImageJ software (W. Rasband, National Institutes of Health, Bethesda, MD). Long time-lapse image sequences were captured using the autofocusing function integrated into the 'advanced time series' macro set (Carl Zeiss MicroImaging). For quantitative FRAP measurements, a 63° – 1.4 NA Plan-Apochromat objective was used. Fluorescence recovery in the bleached region during the time series was quantified using Zeiss LSM software. For presentation purposes, confocal images were exported in TIFF format, and their contrast and brightness optimized in Adobe Photoshop. For FRET analysis, cells were washed three times in PBS, fixed in 2% PFA (Merck) in PBS for 15 min and then washed twice with imaging buffer.

FRET analysis

For acceptor photobleaching FRET, cells were grown on glass coverslips. The cells were fixed by addition of PFA to the medium to a final concentration of 4% for 15 min at room temperature. The cells were washed with PBS containing 1% FCS twice, and then with PBS and mounted onto the microscope. The mCherry-tagged acceptor was photobleached in a ROI over the Golgi complex. The 488-nm or 514-nm laser line was used for the acceptor photobleaching. FRET efficiency (E) was calculated from the CFP-channel images according to:

$$E_F = (\mathrm{F_{post}} - \mathrm{F_{re}})/\mathrm{F_{post}},$$

where F is the intensity of GFP fluorescence using the 488-nm laser before (pre-bleach) and after (post-bleach) photobleaching of mCherry using a high-power 543-nm laser.

Colocalization

Colocalization was performed using the Zeiss colocalization module. Values were obtained after thresholding background pixel values. As control, an image of a cell expressing two fluorescently tagged PLLP variants was used yielding a Pearson's coefficient of 0.98.

Site-directed mutagenesis

Mutagenesis was performed on GFP- and mCherry-tagged PLLP plasmids using the QuickChange (Stratagene) mutagenesis kit. Forward primer sequences are listed: W68A and F71A 5′-CCTATGGCGCGGTGATGG-CCGTCGCTGTCTTC-3′; Y162A and W165A 5′-CTTCTTCAGCGCA-CAGGCCGCCCGAGGAGTAG-3′; W52A 5′-CTGGGGCTGCTGGTG-GCTGCGCTGATTG-3′; F75A 5′-GTTCGTCGCTGTCGCACTCTGGC-TGGT-3′; F119A 5′-CTCTACATCACCGCCGCCATCGCCTGCTCTG-3′; F146A 5′-GCTGCCTCGTTCGCTGCGTGTTTGGTGATG-3′.

Membrane labeling with cholera toxin B subunit (CTXB488)

Cells at 60% confluence in Lab-Tek chambered glass coverslips (NalgeNunc International) were transfected with PLLP–mCherry using FuGENE6 and, after 18 to 24 h, were labeled with 1 µg/ml CTXB488.

Laurdan analysis

COS7 cells were treated with 5 µM Laurdan (Invitrogen, D250) in cell culture medium and incubated for 45 min at 37°C. Subsequently, cells were fixed in 4% PFA and then imaged using a confocal-laser-scanning microscope (SP5; Leica Microsystems) using a 63× glycerol-immersion objective NA 1.3. Laurdan excitation at 780 nm was achieved using a femtosecond-pulsed titanium sapphire laser (Mai-Tai; Spectra-Physics). Laurdan fluorescence was detected simultaneously in two channels of 400–460 nm and 470–530 nm. Generalized polarization (GP) images were constructed using an Image J plugin (Owen and Gaus, 2010). For each pixel, the GP was calculated from the two channel intensity values as:

$$GP = \frac{I_{400-460} - GI_{470-530}}{I_{400-460} + GI_{470-530}},$$

where I represents the intensity in each pixel acquired in the indicated channel, and G is the G-factor or calibration factor. The G factor is then calculated using the following equation:

$$G = \frac{GP_{ref} + GP_{ref}GP_{mes} - GP_{mes} - 1}{GP_{mes} + GP_{ref}GP_{mes} - GP_{ref} - 1}.$$

Here, GP_{mes} is the measured GP value of the reference sample Laurdan in dimethyl sulfoxide (DMSO).

Acknowledgements
Thanks to Ben J. Nichols (MRC Laboratory of Molecular Biology, Cambridge), Miguel A. Alonso (Centro de Biologia Molecular 'Severo Ochoa', Universidad Autonoma de Madrid) and Mikael Simons (Max Planck Institute for Experimental Medicine) for reagents.

Competing interests
The authors declare no competing or financial interests.

Author contributions
Y.Y., I.H., I.N.Y. and J.S. performed experiments. Y.E. helped with confocal microscopy. A.Y. and M.P.C. performed bioinformatics and Rosetta molecular analysis, C.B., A.M. and K.G. performed the Laurdan experiments. Y.E.E. and E.P. performed all the experiments in Schwann cells. K.H. and E.H.S. wrote the manuscript.

Funding
This research was supported by a grant from the German-Israeli Foundation (GIF) for Scientific Research and Development to K.H. and a grant from the Nellie Horwitz foundation to K.H.

Supplementary material
Supplementary material available online at
http://jcs.biologists.org/lookup/suppl/doi:10.1242/jcs.166249/-/DC1

References

Aggarwal, S., Yurlova, L. and Simons, M. (2011a). Central nervous system myelin: structure, synthesis and assembly. *Trends Cell Biol.* **21**, 585-593.
Aggarwal, S., Yurlova, L., Snaidero, N., Reetz, C., Frey, S., Zimmermann, J., Pähler, G., Janshoff, A., Friedrichs, J., Müller, D. J. et al. (2011b). A size barrier limits protein diffusion at the cell surface to generate lipid-rich myelin-membrane sheets. *Dev. Cell* **21**, 445-456.
Aranda, J. F., Reglero-Real, N., Kremer, L., Marcos-Ramiro, B., Ruiz-Saenz, A., Calvo, M., Enrich, C., Correas, I., Millan, J. and Alonso, M. A. (2011). MYADM regulates Rac1 targeting to ordered membranes required for cell spreading and migration. *Mol. Biol. Cell* **22**, 1252-1262.
Boggs, J. M. and Moscarello, M. A. (1978). Dependence of boundary lipid on fatty acid chain length in phosphatidylcholine vesicles containing a hydrophobic protein from myelin proteolipid. *Biochemistry* **17**, 5734-5739.
Bosse, F., Hasse, B., Pippirs, U., Greiner-Petter, R. and Müller, H.-W. (2003). Proteolipid plasmolipin: localization in polarized cells, regulated expression and lipid raft association in CNS and PNS myelin. *J. Neurochem.* **86**, 508-518.
Cochary, E. F., Bizzozero, O. A., Sapirstein, V. S., Nolan, C. E. and Fischer, I. (1990). Presence of the plasma membrane proteolipid (plasmolipin) in myelin. *J. Neurochem.* **55**, 602-610.
Compton, T., Ivanov, I. E., Gottlieb, T., Rindler, M., Adesnik, M. and Sabatini, D. D. (1989). A sorting signal for the basolateral delivery of the vesicular stomatitis virus (VSV) G protein lies in its luminal domain: analysis of the targeting of VSV G-influenza hemagglutinin chimeras. *Proc. Natl. Acad. Sci. USA* **86**, 4112-4116.
Dukhovny, A., Goldstein Magal, L. and Hirschberg, K. (2006). The MAL proteolipid restricts detergent-mediated membrane pore expansion and percolation. *Mol. Membr. Biol.* **23**, 245-257.
Eshed-Eisenbach, Y. and Peles, E. (2013). The making of a node: a co-production of neurons and glia. *Curr. Opin. Neurobiol.* **23**, 1049-1056.
Folch, J. and Lees, M. (1951). Proteolipides, a new type of tissue lipoproteins; their isolation from brain. *J. Biol. Chem.* **191**, 807-817.
Frank, M., van der Haar, M. E., Schaeren-Wiemers, N. and Schwab, M. E. (1998). rMAL is a glycosphingolipid-associated protein of myelin and apical membranes of epithelial cells in kidney and stomach. *J. Neurosci.* **18**, 4901-4913.
Glebov, O. O., Bright, N. A. and Nichols, B. J. (2006). Flotillin-1 defines a clathrin-independent endocytic pathway in mammalian cells. *Nat. Cell Biol.* **8**, 46-54.
Hirschberg, K., Miller, C. M., Ellenberg, J., Presley, J. F., Siggia, E. D., Phair, R. D. and Lippincott-Schwartz, J. (1998). Kinetic analysis of secretory protein traffic and characterization of golgi to plasma membrane transport intermediates in living cells. *J. Cell Biol.* **143**, 1485-1503.
Magal, L. G., Yaffe, Y., Shepshelovich, J., Aranda, J. F., de Marco Mdel, C., Gaus, K., Alonso, M. A. and Hirschberg, K. (2009). Clustering and lateral concentration of raft lipids by the MAL protein. *Mol. Biol. Cell* **20**, 3751-3762.
Miller, A. D., Bergholz, U., Ziegler, M. and Stocking, C. (2008). Identification of the myelin protein plasmolipin as the cell entry receptor for Mus caroli endogenous retrovirus. *J. Virol.* **82**, 6862-6868.
Milovanovic, D., Honigmann, A., Koike, S., Göttfert, F., Pähler, G., Junius, M., Müllar, S., Diederichsen, U., Janshoff, A., Grubmüller, H. et al. (2015). Hydrophobic mismatch sorts SNARE proteins into distinct membrane domains. *Nat. Commun.* **6**, 5984.
Mitra, K., Ubarretxena-Belandia, I., Taguchi, T., Warren, G. and Engelman, D. M. (2004). Modulation of the bilayer thickness of exocytic pathway membranes by membrane proteins rather than cholesterol. *Proc. Natl. Acad. Sci. USA* **101**, 4083-4088.
Naismith, A. L., Hoffman-Chudzik, E., Tsui, L.-C. and Riordan, J. R. (1985). Study of the expression of myelin proteolipid protein (lipophilin) using a cloned complementary DNA. *Nucleic Acids Res.* **13**, 7413-7425.
Nichols, B. J., Kenworthy, A. K., Polishchuk, R. S., Lodge, R., Roberts, T. H., Hirschberg, K., Phair, R. D. and Lippincott-Schwartz, J. (2001). Rapid cycling of lipid raft markers between the cell surface and Golgi complex. *J. Cell Biol.* **153**, 529-542.
Otto, G. P. and Nichols, B. J. (2011). The roles of flotillin microdomains - endocytosis and beyond. *J. Cell Sci.* **124**, 3933-3940.
Owen, D. M. and Gaus, K. (2010). Optimized time-gated generalized polarization imaging of Laurdan and di-4-ANEPPDHQ for membrane order image contrast enhancement. *Microsc. Res. Tech.* **73**, 618-622.
Pérez, P., Puertollano, R. and Alonso, M. A. (1997). Structural and biochemical similarities reveal a family of proteins related to the MAL proteolipid, a component of detergent-insoluble membrane microdomains. *Biochem. Biophys. Res. Commun.* **232**, 618-621.
Presley, J. F., Cole, N. B., Schroer, T. A., Hirschberg, K., Zaal, K. J. and Lippincott-Schwartz, J. (1997). ER-to-Golgi transport visualized in living cells. *Nature* **389**, 81-85.
Rodríguez-Fraticelli, A. E., Bagwell, J., Bosch-Fortea, M., Boncompain, G., Reglero-Real, N., García-León, M. J., Andrés, G., Toribio, M. L., Alonso, M. A., Millan, J. et al. (2015). Developmental regulation of apical endocytosis controls epithelial patterning in vertebrate tubular organs. *Nat. Cell Biol.* **17**, 241-250.
Sal-Man, N., Gerber, D., Bloch, I. and Shai, Y. (2007). Specificity in transmembrane helix-helix interactions mediated by aromatic residues. *J. Biol. Chem.* **282**, 19753-19761.
Sapirstein, V. S., Nolan, C. E., Stadler, I. I. and Fischer, I. (1992a). Expression of plasmolipin in the developing rat brain. *J. Neurosci. Res.* **31**, 96-102.
Sapirstein, V. S., Nolan, C. E., Stern, R., Gray-Board, G. and Beard, M. E. (1992b). Identification of plasmolipin as a major constituent of white matter clathrin-coated vesicles. *J. Neurochem.* **58**, 1372-1378.
Schneider, A., Länder, H., Schulz, G., Wolburg, H., Nave, K.-A., Schulz, J. B. and Simons, M. (2005). Palmitoylation is a sorting determinant for transport to the myelin membrane. *J. Cell Sci.* **118**, 2415-2423.
Simons, M., Krämer, E. M., Macchi, P., Rathke-Hartlieb, S., Trotter, J., Nave, K.-A. and Schulz, J. B. (2002). Overexpression of the myelin proteolipid protein leads to accumulation of cholesterol and proteolipid protein in endosomes/lysosomes: implications for Pelizaeus-Merzbacher disease. *J. Cell Biol.* **157**, 327-336.
Thomas, D. C., Brewer, C. B. and Roth, M. G. (1993). Vesicular stomatitis virus glycoprotein contains a dominant cytoplasmic basolateral sorting signal critically dependent upon a tyrosine. *J. Biol. Chem.* **268**, 3313-3320.
Van Dorsselaer, A., Nebhi, R., Sorokine, O., Schindler, P. and Luu, B. (1987). [The DM-20 proteolipid is a major protein of the brain. It is synthetized in the fetus earlier than the major myelin proteolipid (PLP)]. *C. R. Acad. Sci. III* **305**, 555-560.
van Meer, G. and Simons, K. (1982). Viruses budding from either the apical or the basolateral plasma membrane domain of MDCK cells have unique phospholipid compositions. *EMBO J.* **1**, 847-852.
Yaffe, Y., Shepshelovitch, J., Nevo-Yassaf, I., Yeheskel, A., Shmerling, H., Kwiatek, J. M., Gaus, K., Pasmanik-Chor, M. and Hirschberg, K. (2012). The MARVEL transmembrane motif of occludin mediates oligomerization and targeting to the basolateral surface in epithelia. *J. Cell Sci.* **125**, 3545-3556.
Yurlova, L., Kahya, N., Aggarwal, S., Kaiser, H.-J., Chiantia, S., Bakhti, M., Pewzner-Jung, Y., Ben-David, O., Futerman, A. H., Brügger, B. et al. (2011). Self-segregation of myelin membrane lipids in model membranes. *Biophys. J.* **101**, 2713-2720.
Zaal, K. J., Smith, C. L., Polishchuk, R. S., Altan, N., Cole, N. B., Ellenberg, J., Hirschberg, K., Presley, J. F., Roberts, T. H., Siggia, E. et al. (1999). Golgi membranes are absorbed into and reemerge from the ER during mitosis. *Cell.* **99**, 589-601.

Journal of Cell Science

Supplemental movies legend

Movie1. VSVG accumulation around the Golgi in PLLP expressing cells. Co-expression of VSVG-YFP (green) and PLLP-mCherry (red) in COS7 cells. Cells were imaged after overnight incubation at 39.5°C to accumulate VSVG in the ER and shift to 32 °C.

Movie2. PLLP blocks VSVG secretory transport. Co-expression of VSVG-YFP (inverted right hand side of movie) and PLLP-mCherry (left hand side of movie) in COS7 cells.

Movie3. PLLP does not blocks VSVGIn4 secretory transport. Co-expression of VSVGIn4-YFP (green and inverted right hand side of movie) and PLLP-mCherry (red left hand side of movie) in COS7 cells.

Figure S1. Analysis of relative colocalizations of PLLP-mCherry, VSVG-CFP and VSVGIn4-YFP. A. Cells were cotransfected with PLLP-mCherry, VSVG-CFP and VSVGIn4-YFP and incubated overnight at 39.5 °C. Cells were than shifted to 32°C and images were captured at 20 sec intervals for about 90 min. **B.**Pearson's coefficient was determined in images at the designated times throughout the experiment. Coefficient was determined for the Golgi area only.

Movie 1.

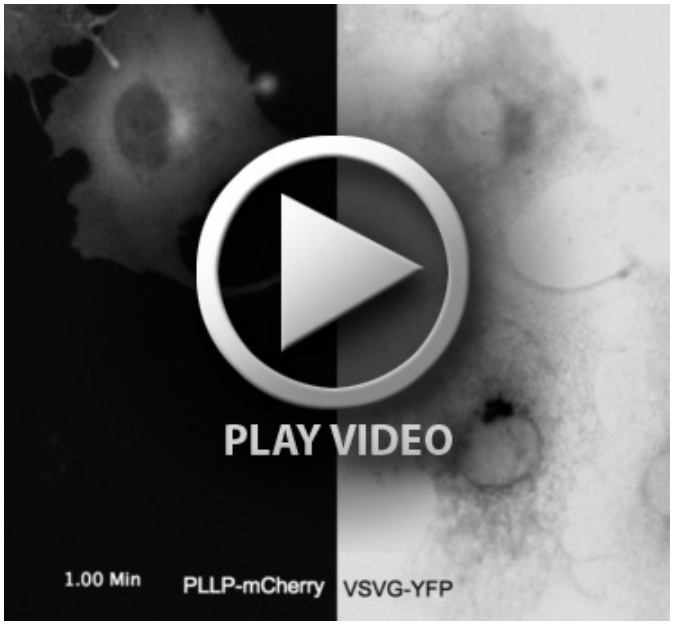

Movie 2.

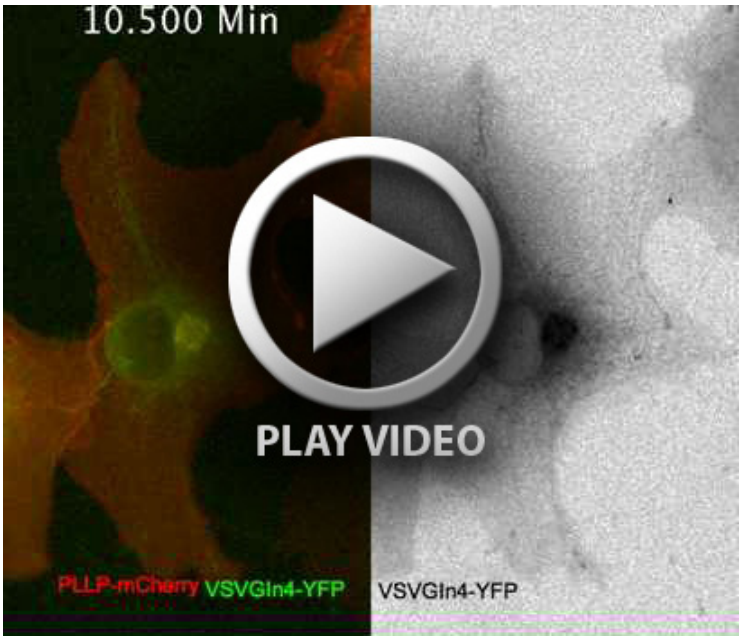

Movie 3.

Figure S1

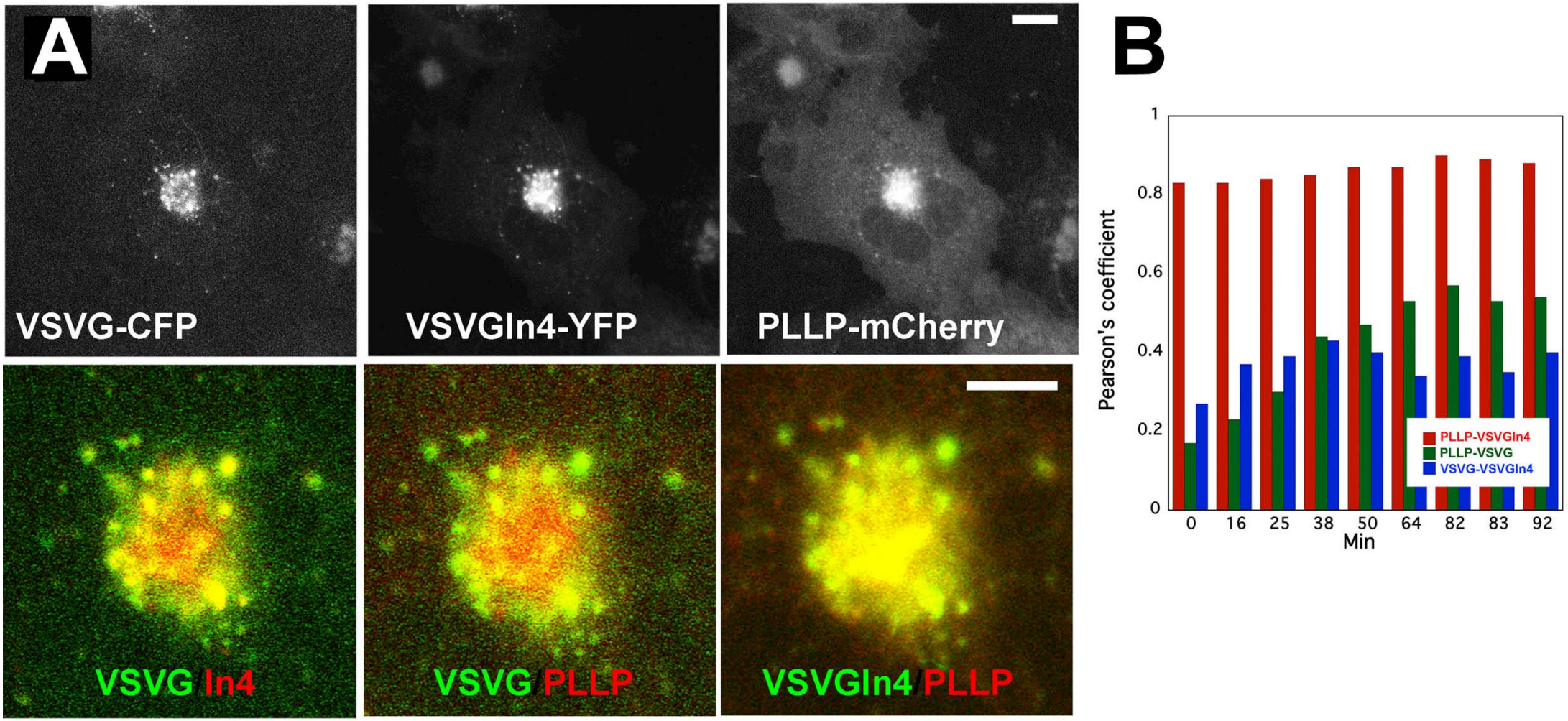
A
VSVG-CFP
VSVGIn4-YFP
PLLP-mCherry
VSVG In4
VSVG PLLP
VSVGIn4 PLLP
B
Pearson's coefficient
1
0.8
0.6
0.4
0.2
0
0
16
25
38
50
64
82
83
92
Min
PLLP-VSVGIn4
PLLP-VSVG
VSVG-VSVGIn4